

Broad gain bandwidth injectorless quantum-cascade lasers with a step well design

H. Li,^{a)} Simeon Katz, Gerhard Boehm, and Markus-Christian Amann

Walter Schottky Institut, Technische Universität München, Am Coulombwall 3, D-85748 Garching, Germany

(Received 27 January 2011; accepted 9 March 2011; published online 31 March 2011)

The authors present a broad gain bandwidth injectorless quantum-cascade laser (QCL) with a “short period superlattice” design which provides an equivalent GaInAlAs alloy quantum step well in each active module. Devices employing the proposed step well design demonstrate an ultrabroadband gain spectrum of 480 cm^{-1} ($\sim 4\text{ }\mu\text{m}$) around the threshold at room temperature in pulsed mode. The fabricated $30\text{ }\mu\text{m}$ wide and 4 mm long laser shows the lowest room temperature threshold current density of 1.1 kA/cm^2 among the broad gain QCLs emitting at similar wavelengths and a high slope efficiency of 1.6 W/A at room temperature in pulsed mode. © 2011 American Institute of Physics. [doi:10.1063/1.3571562]

Quantum-cascade lasers (QCLs) have experienced significant improvements in operating temperature, threshold, wall-plug efficiency, output power, and wavelength coverage within the last decade.^{1–5} The rapid progress of QCLs is attributed to the advances in semiconductor technology and the full use of band engineering. Besides the device parameters mentioned above, the pursuit of a broad gain bandwidth which is proportional to the full width at half maximum (FWHM) value of the electroluminescence (EL) spectrum has attracted much interest recently. Though a broad gain width may spoil the output power and the threshold of lasers, it is also required for wide tuning applications by using external cavity, distributed feedback laser array technology, and so on.⁶

Different approaches have been used to achieve broad gain bandwidth for QCLs, such as multiple stacks of bound-to-continuum active regions,⁷ continuum-to-bound transition,⁸ dual upper state design,⁹ continuum-to-continuum transition,⁶ and dual upper state to multiple-lower-state transition,¹⁰ etc. At present, the achieved broadest gain spectrum for QCLs is 500 cm^{-1} with a peak emission wavelength around $8.7\text{ }\mu\text{m}$. In this letter, we propose an injectorless QCL based on a step well design which produces a broad gain bandwidth of 480 cm^{-1} around the threshold at room temperature in pulsed mode with the lasing wavelength around $8.6\text{ }\mu\text{m}$, a low room temperature threshold current density of 1.1 kA/cm^2 , and a high room temperature slope efficiency of 1.6 W/A .

Figure 1 shows the band structure of the QCL active region based on a strain balanced four-alloy double-phonon-resonance design,³ employing AlAs as a blocking layer and InAs for the optical transition enhancement, at an electric field of 81 kV/cm . This design is featured by the three pairs of GaInAs/AlInAs “short period superlattice” structure in each period. Because the individual layer thickness in the superlattice structure, 0.33 or 0.22 nm for AlInAs or GaInAs, respectively, is close to or even smaller than a single monolayer, the superlattice structure actually forms an equivalent alloy GaInAlAs quantum step well in each period. The barrier height of the quantum step well is schematically indi-

cated by a slash in each period as shown in Fig. 1. Such step well design has the following advantages: (1) it lowers the barrier height between the quantum states located in the adjacent quantum wells A and B. Also note that the majority of electrons in state 2 resides in quantum well A and the dipole matrix element between states 4 and 2, z_{42} , is about a half of z_{43} ; therefore, the optical transition between states 4 and 2 is made possible besides the natural optical transition between 4 and 3 in this design. The energy spacing between 3 and 2 is 34 meV corresponding to a longitudinal optical phonon energy. This double-lower-state design leads to a broad gain spectrum. (2) Because of the wide step well structure (1.59 nm), the optical transition here can be designed more diagonally and, therefore, the upper lifetime τ_4 could be much longer than other designs. The device threshold may benefit from the long upper lifetime.

The QCL active region was grown by a solid source molecular beam epitaxy on a InP substrate doped to $2 \times 10^{17}\text{ cm}^{-3}$. The growth started with a 500 nm thick lattice matched GaInAs cladding layer ($6 \times 10^{16}\text{ cm}^{-3}$), followed

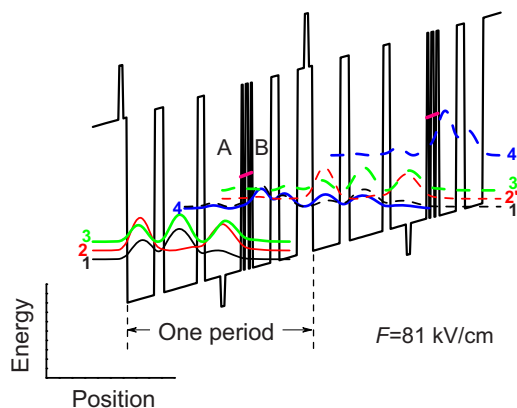


FIG. 1. (Color online) Conduction band structure and the moduli squared of the wave functions of the “short period superlattice” active region at an electric field of 81 kV/cm . The layer sequence of one period, from right to left, is **0.6/0.5/1/2.8/1.1/2.5/0.33/0.2/0.33/0.2/0.33/2.4/0.51/2.4/1/4.9/1.3/3.9** nm, where **AlInAs** layers are in **bold**, **AlAs** in **bold italic**, **InAs** in **italic**, **GaInAs** in normal font, and the underlined layers are doped to $5.1 \times 10^{16}\text{ cm}^{-3}$ corresponding to a sheet density of $4.5 \times 10^{10}\text{ cm}^{-2}$. The slash in the “short period superlattice” area schematically indicates the barrier height of the equivalent GaInAlAs quantum step well.

^{a)}Electronic mail: hua.li@wsi.tum.de.

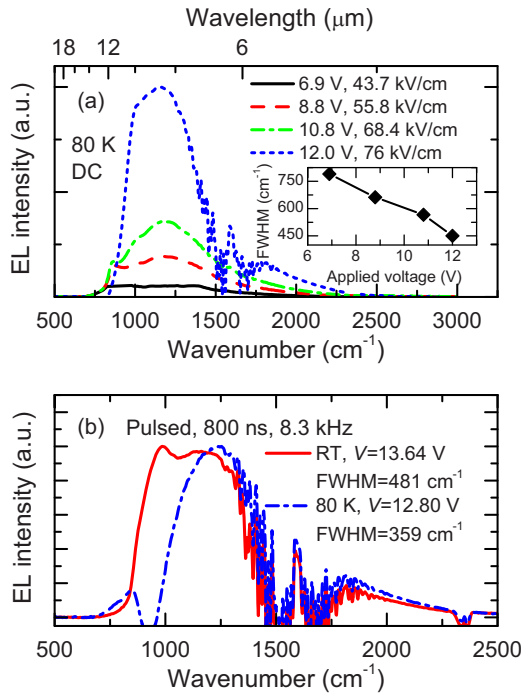


FIG. 2. (Color online) Intersubband EL spectra of a 22 μm wide and 2 mm long device at various applied voltages. All data are collected at a heat sink temperature of 80 K in dc operation. The inset shows the bandwidth, FWHM, of the spectra as a function of applied voltage. (b) EL spectra around thresholds recorded at both low temperature (80 K) and room temperature in pulsed mode.

by the active region core. The active region comprises 60 periods strain balanced $\text{Ga}_{0.4}\text{In}_{0.6}\text{As}/\text{Al}_{0.635}\text{In}_{0.365}\text{As}$ layers with a total thickness of 1.6 μm . Then, another GaInAs upper cladding layer doped to $6 \times 10^{16} \text{ cm}^{-3}$ was grown above the active region. The upper waveguide consists of a 2.7 μm InP doped to $6 \times 10^{16} \text{ cm}^{-3}$ and a 1 μm GaInAs plasmon layer doped to $5 \times 10^{18} \text{ cm}^{-3}$, which was finally capped with a 200 nm GaInAs contact layer doped to $1 \times 10^{19} \text{ cm}^{-3}$. After the growth, the sample was processed into ridge lasers with a width between 22 and 30 μm by using wet etching. After the top and bottom contact evaporations, the as-cleaved laser bars between 2–4 mm cavity lengths were mounted on a cooper heat sink for measurements. The power of the fabricated lasers were measured using a calibrated thermopile detector and the threshold was recorded by a more sensitive liquid nitrogen cooled mercury-cadmium-telluride (MCT) detector. A Bruker Fourier transform infrared spectrometer was used to measure the EL and lasing spectra.

Figure 2(a) shows the intersubband EL spectra of an as-cleaved 22 μm wide and 2 mm long device at 80 K in dc operation at different applied voltages. The precise alignment and a much longer integration time are required for measuring the small intersubband spontaneous emission (in nanowatts power level¹¹). A single dominant peak around 1155 cm^{-1} is clearly observed over the whole bias range. The bandwidth or the FWHM measured from the EL spectra as a function of applied voltage is plotted in the inset of Fig. 2. The FWHM value decreases from 790 to 450 cm^{-1} with increasing applied voltage (electric field) from 6.9 (43.7) to 12 V (76 kV/cm). To exclude the effects from the black body radiation and stimulated emission, we also measured the spontaneous EL spectra around thresholds in pulsed mode as shown in Fig. 2(b). At 80 K the EL FWHM is about

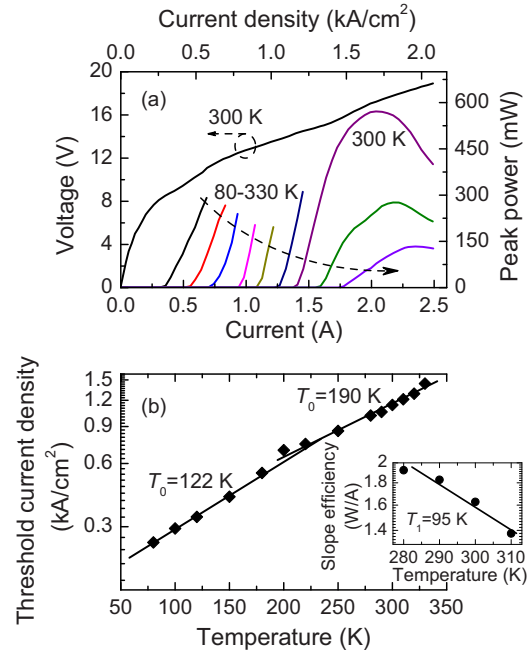


FIG. 3. (Color online) (a) Measured L - I - V characteristics of a 30 μm wide and 4 mm long laser operating in pulsed mode at different heat sink temperatures. (b) Threshold current density as a function of heat sink temperature. The inset shows the slope efficiencies of the laser around room temperature range.

360 cm^{-1} , while the room temperature EL spectrum shows a much wider bandwidth of 480 cm^{-1} ($\sim 59 \text{ meV}$) due to the level broadening effect. The ultrabroad gain bandwidth is attributed to the double radiative transitions because of the step well design.

The light-current-voltage (L - I - V) characteristics of a laser with a ridge width of 30 μm and a cavity length of 4 mm over various heat sink temperatures are shown in Fig. 3(a). The curves were recorded in pulsed mode with a 500 ns pulse width and a 250 Hz repetition rate. The lasing is observed up to 350 K and at room temperature the output pulse power is 570 mW. Figure 3(b) shows the threshold current density as a function of temperature. By fitting the threshold to an empirical formula, the characteristic temperature T_0 shows two values, i.e., 122 K in low temperature range and 190 K around room temperature. To fully evaluate the temperature performance of the laser, we also plot the slope efficiency around room temperature in the inset of Fig. 3(b) which gives the characteristic temperature $T_1=95 \text{ K}$. Though T_0 and T_1 are not as large as those of some other high performance QCLs, the room temperature threshold and slope efficiency show excellent values. At 300 K, the threshold current density is as low as 1.1 kA/cm^2 which is the lowest among the broad gain QCLs emitting at the similar wavelengths and the slope efficiency reaches 1.6 W/A. Regarding the low threshold current density presented here, we have the following explanations: (1) compared to the conventional injector-based QCL, the injectorless QCL has a much shorter period length (nearly half of the period of the injector-based QCL). To give a similar confinement factor, the active region thickness of our structure is kept same with that of the injector-based QCL. The shorter period length and the similar active region thickness result in a larger number of cascade stages in our design which then leads to the low threshold current density.¹² (2) No injection miniband is used

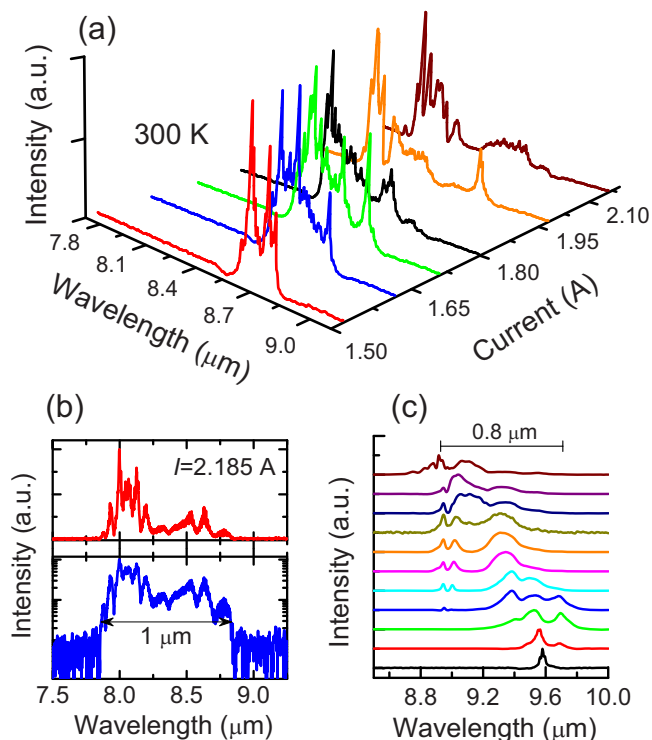


FIG. 4. (Color online) (a) Normalized emission spectra of the broad gain bandwidth laser as a function of drive current at room temperature. (b) High resolution emission spectrum at a drive current of 2.185 A in linear (upper panel) and logarithmic (lower panel) scales at room temperature. (c) Emission spectra of another similar step well QCL with a lattice matched material design as a function of drive current at cryogenic temperature. The current increases from bottom to top. The spectra intensity is normalized and shifted vertically for clarity.

in our injectorless QCLs, the intraminiband and intersubband absorption losses are largely reduced. Given a same gain value, the injectorless design gives a lower threshold. In addition, the long upper state lifetime and the adoption of lower doping concentration in the active region also contribute to the low threshold current density.^{13,14} Though the threshold is low, the high operating voltage and the small dynamic range shown in Fig. 3 limit the laser performance, such as the output power and the continuous wave operation. Therefore, further optimizations in number of the periods and doping are potential to improve the performance of the broad gain QCL.

Figure 4(a) shows the lasing spectra of the 30 μm wide and 4 mm long step well QCL measured at room temperature in pulsed mode (500 ns pulse and 10 kHz frequency) over various drive currents. As the current is increased, the lasing spectrum covers a broader and broader wavelength range. When the current reaches 1.8 A or higher, a spectrum covering 1 μm wavelength range is obtained. Figure 4(b) shows the high resolution spectra at a typical current of 2.185 A. Continuous Fabry-Pérot modes from 7.85 to 8.85 μm are clearly seen. The broad Fabry-Pérot spectrum obtained using

the step well design is not an accident phenomenon. In Fig. 4(c), we plot the emission spectra measured from a similar step well QCL with a lattice matched GaInAs/AlInAs active region design emitting around 9 μm at cryogenic temperature. Over the entire current range, the lasing spectra also spread a broad wavelength range of 0.8 μm . The broad emission spectrum is definitely another proof of broad gain besides the broad spontaneous EL spectrum. However, it is worth noting that the inhomogeneous broad emission spectra at high drive currents due to the coherent instabilities^{9,15} may hinder the single mode operation under wavelength tuning.

In conclusion, we have presented broad gain bandwidth injectorless QCLs with a quantum step well active region design. The measured intersubband EL spectra exhibit an ultrabroad bandwidth of 480 cm^{-1} ($\sim 4 \mu\text{m}$) around the threshold at room temperature. The fabricated ridge lasers show a low threshold current density of 1.1 kA/cm^2 and a high slope efficiency of 1.6 W/A at room temperature. The measured room temperature emission spectra also demonstrate a broad and continuous Fabry-Pérot modes lasing from 7.85 to 8.85 μm . The external cavity tuning and related applications of the broad gain injectorless QCLs are proposed for the future work.

One of the authors (H.L.) would like to acknowledge the support from the Alexander von Humboldt foundation. This work was supported by the German excellence cluster “Nanosystems Initiative Munich (NIM).”

- ¹J. Faist, F. Capasso, D. L. Sivco, C. Sirtori, A. L. Hutchinson, and A. Y. Cho, *Science* **264**, 553 (1994).
- ²M. Razeghi, S. Slivken, Y. B. Bai, B. Gokden, and S. R. Darvish, *New J. Phys.* **11**, 125017 (2009).
- ³S. Katz, G. Boehm, and M. C. Amann, *Electron. Lett.* **44**, 580 (2008).
- ⁴H. Li, S. Katz, A. Vizbaras, G. Boehm, and M. C. Amann, *IEEE Photonics Technol. Lett.* **22**, 1811 (2010).
- ⁵C. Walther, M. Fischer, G. Scalari, R. Terazzi, N. Hoyler, and J. Faist, *Appl. Phys. Lett.* **91**, 131122 (2007).
- ⁶Y. Yao, X. J. Wang, J. Y. Fan, and C. F. Gmachl, *Appl. Phys. Lett.* **97**, 081115 (2010).
- ⁷C. Gmachl, D. L. Sivco, R. Colombelli, F. Capasso, and A. Y. Cho, *Nature (London)* **415**, 883 (2002).
- ⁸Y. Yao, W. O. Charles, T. Tsai, J. X. Chen, G. Wysocki, and C. F. Gmachl, *Appl. Phys. Lett.* **96**, 211106 (2010).
- ⁹K. Fujita, T. Edamura, S. Furuta, and M. Yamanishi, *Appl. Phys. Lett.* **96**, 241107 (2010).
- ¹⁰K. Fujita, S. Furuta, T. Dougakiuchi, A. Sugiyama, T. Edamura, and M. Yamanishi, *Opt. Express* **19**, 2694 (2011).
- ¹¹J. Faist, F. Capasso, C. Sirtori, D. Sivco, A. L. Hutchinson, S. N. G. Chu, and A. Y. Cho, *Appl. Phys. Lett.* **64**, 1144 (1994).
- ¹²C. Gmachl, F. Capasso, A. Tredicucci, D. L. Sivco, R. Kohler, A. L. Hutchinson, and A. Y. Cho, *IEEE J. Sel. Top. Quantum Electron.* **5**, 808 (1999).
- ¹³J. Faist, *Appl. Phys. Lett.* **90**, 253512 (2007).
- ¹⁴T. Aellen, M. Beck, N. Hoyler, M. Giovannini, J. Faist, and E. Gini, *J. Appl. Phys.* **100**, 043101 (2006).
- ¹⁵C. Y. Wang, L. Diehl, A. Gordon, C. Jirauschek, F. X. Kartner, A. Belyanin, D. Bour, S. Corzine, G. Hoffer, M. Troccoli, J. Faist, and F. Capasso, *Phys. Rev. A* **75**, 031802 (2007).